Available online at www.sciencedirect.com
SCIENCE DIRECT
Journal of Molecular Catalysis A: Chemical 253 (2006) 252–260
JOURNAL OF MOLECULAR CATALYSIS A: CHEMICAL
www.elsevier.com/locate/molcata

Synthesis and characterization of xerogel titania modified with Pd and Ni

L.M. Martínez T[a], C. Montes de Correa[a,*], J.A. Odriozola[b], M.A. Centeno[b]

[a] *Departamento de Ingeniería Química, Universidad de Antioquia, A.A 1226, Medellín, Colombia*
[b] *Departamento de Química Inorgánica e Instituto de Ciencia de Materiales de Sevilla, Universidad de Sevilla-CSIC, Avda. Américo Vespucio 49, 41092 Sevilla, Spain*

Received 24 January 2006; received in revised form 18 March 2006; accepted 20 March 2006
Available online 2 May 2006

Abstract

Pd and Ni supported on TiO_2 have been synthesized by the sol–gel method and characterized by X-ray diffraction (XRD), X-ray fluorescence (XRF), N_2 sorption, TGA–DTG, TEM and NH_3-TPD with DRIFTS. Catalyst samples were also examined in the oxidative destruction of dichloromethane (DCM) in the presence of water vapor. Acid hydrolysis of titania precursor was performed with H_2SO_4 or HNO_3 as hydrolysis catalysts and two procedures were used for modifying titania with Pd or Ni, namely impregnation and cogellation. Sulphated catalysts exhibited higher surface area, average pore diameter and total pore volume than those prepared with HNO_3. Brönsted acid sites created by sulphate species anchored on titania favored extraction of Cl atoms from DCM molecule. DCM oxidation was much higher over sulphated catalysts as compared to un-sulphated ones, catalysts prepared by impregnation exhibited higher activity than those prepared by cogellation and Pd was more effective than Ni for burning-off coke deposited over support surface. Pd impregnated on sulphated xerogel titania was the most selective catalyst to CO_2 and HCl. Therefore, bifunctional catalysts, i.e. containing palladium and Brönsted acid sites are required for total combustion of DCM at relatively low temperatures.

Keywords: Sol–gel process; Titania; Palladium; Nickel; Dichloromethane oxidation; Impregnated catalysts; Cogelled catalysts

1. Introduction

Titanium dioxide is a versatile material used as pigment, catalyst, filler, coating, photoconductor, UV filter, etc. As catalyst, it exhibits a number of attractive characteristics such as chemical stability, non-toxicity, low cost and high oxidation rates [1]. TiO_2 has the additional advantage of being biocompatible, environmentally friendly, and readily available. Titanium dioxide has two commercially important crystal structures: rutile and anatase. Titania-anatase has been extensively used as catalyst support [1,2]. However, there are some disadvantages associated with titania-anatase which include low specific surface area, poor thermal stability, phase transformation from anatase to thermodynamically stable rutile form, poor mechanical strength, and lack of abrasion resistance. Therefore, much effort has been made in recent years to develop new catalyst formulations, which can enhance the thermal (textural) stability of TiO_2 without loosing its unique physicochemical properties. Lately, the sol–gel method has been widely used to prepare a large variety of catalysts with tailored properties. The surface properties of sol–gel titania can be further modified in conjunction with noble or transition metals as promoters. When noble metals are introduced in a sol–gel titania or a second metal oxide doped titania, high activity for NO reduction or CO oxidation is observed [3]. Usually, a weak or strong interaction between supported noble metal and titania may occur [4] depending on reduction temperature and preparation method. This interaction strongly affects not only the surface reduction properties and acid–basic character, but the catalytic activity also. Additionally, strong acidic sites on titania prepared with sulphuric acid, i.e. sulphated titania, ST, develop the ability to catalyze reactions characteristic of very strong acid catalysts at low temperatures [5]. Sulphated TiO_2 ($H_0 < -11.93$) is sufficiently stable at elevated reaction temperatures and conveniently regenerated [1]. In the present study we examine the effect of preparation, namely use of nitric acid versus sulphuric acid and impregnation versus cogellation, on physicochemical characteristics and reactivity of selected sol–gel titania catalysts modified with Pd or Ni.

* Corresponding author. Tel.: +57 4 2106605; fax: +57 4 2106609.
E-mail addresses: cmontes@udea.edu.co, cmontes@quimbaya.udea.edu.co (C. Montes de Correa).

1381-1169/$ – see front matter © 2006 Elsevier B.V. All rights reserved.
doi:10.1016/j.molcata.2006.03.052

2. Experimental

2.1. Catalyst preparation

Catalysts were prepared following previously reported procedures [6–8]. The unmodified support was prepared dissolving 5.0 mL of titanium butoxide (Acros) in 33.5 mL of cyclohexene (Mallinckrodt) at 333 K (solution A). A second solution (solution B) containing 3.2 mL of H_2O and 0.16 mL of sulfuric acid (Cadearbo) or 0.12 mL of nitric acid (J.T. Baker) were added dropwise into solution A until gelation. Acid medium favors alcoxide hydrolysis and condensation reaction generated by water. Finally, gel was aged 24 h at 276 K without stirring. The solvent was evaporated at room temperature, and recovered solid was dried in an oven at 373 K for 1 day and calcined at 873 K during 4 h. Sulphated and un-sulphated catalysts are coded ST and UST, respectively.

Cogelled sulphated titania modified with Pd or Ni catalysts were prepared following the above procedure but, 0.017 g of palladium acetyl acetonate (Merck, Aldrich) or 0.024 g of nickel acetyl acetonate (Merck, Aldrich) were dissolved in solution B prior to mixing solutions A and B. The resulting solids were then dried at 373 K for 1 day. Pd loaded samples were calcined at 573 K for 1 h, while Ni loaded samples were calcined at 623 K during 1 h. The nominal metal composition of synthesized catalysts, PdST(C) and NiST(C), was 0.5 wt.%.

Impregnated catalysts were prepared as follows: 0.0144 g of palladium acetyl acetonate (Merck, Aldrich) or 0.0231 g of nickel acetyl acetonate (Merck, Aldrich), diluted in 4.0 mL of cyclohexene were added to powdered sulphated TiO_2 (ST) to obtain a metal loading of 0.5 wt.%. The resulting solids were then dried at 373 K for 1 day. Pd loaded samples were calcined at 573 K for 1 h, while Ni loaded samples were calcined at 623 K during 1 h. Sulphated catalysts modified by impregnation are coded PdST(I), NiST(I) and impregnated un-sulphated ones: PdUST(I), NiUST(I).

2.2. Catalyst characterization

Chemical composition of catalysts was determined by X-ray fluorescence (XRF) in a Siemens SRS 3000 sequential spectrophotometer equipped with a rhodium tube. XRF measurements were performed onto pressed pellets (sample included in 10 wt.% of wax). The XRF apparatus was previously calibrated from references of known compositions of Si, P and Cs, these references being mixtures of SiO_2, CaP_2O_7 and Cs_2CO_3.

A Seiko Exstar 6300 thermal analysis instrument was used for studying thermal evolution of catalyst precursors. Samples were heated from room temperature to 1073 K at a heating rate of 10 K min^{-1} under static air.

Nitrogen adsorption–desorption isotherms were measured at 77 K over a relative pressure range from 0.01 to 0.995, using an ASAP 2010 system manufactured by Micromeritics. Prior to adsorption experiments, catalyst samples were degassed under a vacuum of 10^{-3} Torr for 2 h at 423 K. Specific surface areas were measured using BET method, being reproducible within ±5%. Pore diameter and pore size distribution were determined by the BJH method and the existence of microporosity tested from *t*-plot constructions.

X-ray diffraction (XRD) studies were carried out on a Philips PW 1710 X-ray diffractometer using Cu Kα radiation and Ni filter. The X-ray tube was operated at 30 kV and 20 mA. Samples were scanned from $2\theta = 10°$–$80°$ ($\Delta\theta = 0.05°$, $\zeta = 2.5$ s). The proportion of each phase was calculated using Eq. (1) [9].

$$\%\text{Anatasephase} = \frac{I(\text{Max, anatasephase})}{I(\text{Max, anatasephase}) + I(\text{Max, rutilephase})} \times 100 \quad (1)$$

where I(Max, anatase phase) accounts for the maximum intensity of characteristic peak.

Crystal sizes were calculated using the Scherrer equation [10]:

$$t = \frac{0.9\lambda}{B\,\text{Cos}\,\theta} \quad (2)$$

where t = crystal particle diameter (Å), λ = wavelength (Å), B = broadening of diffraction line measured at half its maximum intensity (radians) and θ = reflection angle (radians).

Transmission electron microscopy (TEM) observations were carried out in a Philips CM200 microscope with dispersive X-ray analysis (EDX). Samples were dispersed in ethanol by sonication and dropped on a copper grid coated with a carbon film.

Diffuse reflectance infrared spectra (DRIFTS) were collected for samples placed in a controlled DRIFTS chamber with SeZn windows and coupled to a Thermo Nicolet Nexus infrared spectrometer using KBr optics and a MCT/B detector working at liquid nitrogen temperature, as we previously reported [11]. Prior to adsorption, catalysts were pretreated for 1 h in flowing 2000 ppm NH_3/He calibrated mixture (Abelló Linde). Afterwards, helium was allowed to flow during 1 h in order to desorb loosely bound ammonia species. Once these NH_3 were purged the acidity of the resulting catalysts was analyzed by heating the solids under He flow at 50 K intervals from 373 to 773 K. Spectra shown resulted from subtraction of spectra recorded at temperature T and those recorded at room temperature so small features usually hidden in the raw spectra may be observed and analyzed.

2.3. Catalytic tests

Catalytic experiments were performed in a fixed bed pyrex tubular reactor at atmospheric pressure. Heated teflon tubing was used from reactor to gas analyzer to prevent metal wall mediated reactions and product condensation. Prior to each reaction catalyst samples were pretreated in flowing 5% H_2/He while being heated at a rate of 2 K min^{-1} up to 573 K for Pd and 623 K for Ni catalysts and then held at this temperature during 1 h. For a typical reaction, a catalyst weight of 100 mg (particle sizes in the range 250–425 μm) and a total flow of 20 mL/min of a gas stream containing 1945 ppm CH_2Cl_2, 4.8% O_2, 1% H_2O and He (balance) was used. The space velocity was 0.005 g min mL^{-1}. Catalysts were stabilized in the reaction mixture at room temperature. After getting stable DCM concen-

trations (1–3 h), reaction temperature was increased up to 773 K and composition of effluent gases monitored by FTIR (TEMET) under steady state conditions (4 h at the selected reaction temperature). The analysis technique allows quantification of all reactants and products present in the gas phase having a dipolar moment different from zero. Diatomic molecules like Cl_2 and H_2 cannot be observed but chloromethanes, carbon oxides, partial oxidation products as CH_3OH, HCHO or HCOOH, HCl and H_2O or even phosgene might be detected. These compounds have been previously monitored in the oxidation of DCM [7,12]. However, in our case a careful study of the gas phase IR spectra under steady state reaction conditions at the studied reaction temperatures let us state only the presence of DCM, CO_x, HCl and H_2O in the gas phase. Products of interest like Cl_2 and H_2 that might be present as a result of primary or secondary reactions cannot be observed.

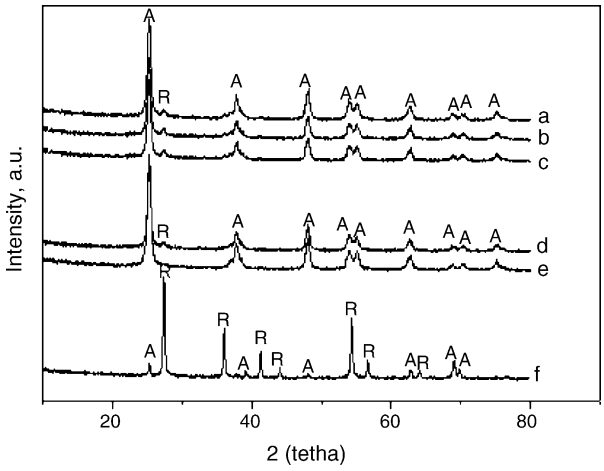

Fig. 1. XRD patterns of xerogel titania catalysts. (a) ST; (b) PdST(I); (c) NiST(I); (d) PdST(C); (e) NiST(C); (f) UST. A: anatase; R: rutile.

3. Results and discussion

3.1. Characterization

3.1.1. Crystalline phases

Fig. 1 shows X-ray diffraction patterns of ST, PdST(I), NiST(I), PdST(C) and NiST(C), as well as, that of UST. No additional phases from palladium or nickel oxides were observed in the XRD patterns indicating that Pd and Ni phases were highly dispersed or metal loading was quite low for sensitivity limits of this technique. As can be observed in Table 1, crystal structure of ST, was mainly anatase (90% anatase, 10% rutile). Only a slight change in phase composition of ST could be detected by impregnation with Pd (87% anatase, 13% rutile) or nickel (88% anatase, 12% rutile) but, pure anatase phase was favoured by the addition of precursor salts during gellation, i.e. cogelled catalysts (see Table 1). In contrast rutile form became dominant in sol-gel UST (9% anatase, 91% rutile). As can be observed in Fig. 1, characteristic peaks of anatase phase are $2\theta = 25.38^\circ$, 37.7°, 48.2°, 54.1° and 55.0°. On the other hand, peaks at $2\theta = 27.4^\circ$, 35.9° and 54.3° are typical of rutile. For the sake of comparison, application of Scherrer equation see Eq. (2) allowed us to establish a crude estimate of crystallite sizes. UST has a larger crystallite size (34.5 nm) than ST (30 nm). This is consistent with previous observations indicating that crystallite size decreases in the presence of sulphate ions as SO_4^{2-} species could possibly interact with TiO_2 network, and thus hinder particle growth [13]. Even a very small amount of SO_4^{2-} species is responsible for this effect. PdST(I) and NiST(I) have the same average crystal size (27.1 nm), while crystal size of PdST(C) is 24.9 nm and that of NiST(C) is 17.1 nm. Note that smaller crystallite sizes in cogelled materials as compared to impregnated ST samples maybe ascribed to pretreatment conditions, 1 h at 573 K and 623 K for PdST(C) and NiST(C), respectively. On the other hand, ST samples were calcined at 873 K before impregnation with Pd or Ni.

3.1.2. Textural properties

Table 1 also compiles BET surface area, pore volume and average pore diameter for both cogelled and impregnated Ni and Pd modified sulphated titania samples and for a UST sample. Results of N_2 adsorption in Table 1 show that surface area of UST was quite low after calcination at 873 K compared to that of ST calcined at the same temperature. Therefore, sulphation greatly retarded ST sintering. Surface areas are practically constant when fresh ST is modified by the addition of Pd or Ni acetylacetonate either by impregnation or cogellation. Fig. 2 shows nitrogen adsorption isotherms for UST, ST and PdST(I). The shape of adsorption isotherms (nitrogen adsorbed volume versus relative pressure) depends on catalyst porous texture. As can be observed in Fig. 2, isotherms did not significantly change for ST supported catalysts, while for the same relative pressures, UST showed lower adsorbed V_{N2}. This catalyst has lower pore

Table 1
Physicochemical properties of xerogel titania supported catalysts

Sample	XRD		N_2 isotherms				XRF		
	%A	CS (nm)	S_{BET} ($m^2\,g^{-1}$)	V ($cm^3\,g^{-1}$)	D (nm)	Mp ($m^2\,g^{-1}$)	Pd	Ni	S
ST	89.77	29.94	84	0.33	15.9	0.8	–	–	0.8
PdST(I)	86.78	27.10	77	0.33	17.6	6	0.337	–	0.763
NiST(I)	88.06	27.10	79	0.37	18.6	6.1	–	0.556	0.704
PdST(C)	94.16	24.88	73	0.33	18.2	1.5	0.359	–	0.741
NiST(C)	100	17.05	83	0.41	19.9	24.4	–	0.426	–
UST	8.9	34.51	2.66	0.007	10.7	0.97	–	–	–

% A: % anatase phase; CS: crystal size; V: pore volume; D: pore diameter; Mp: micropore area.

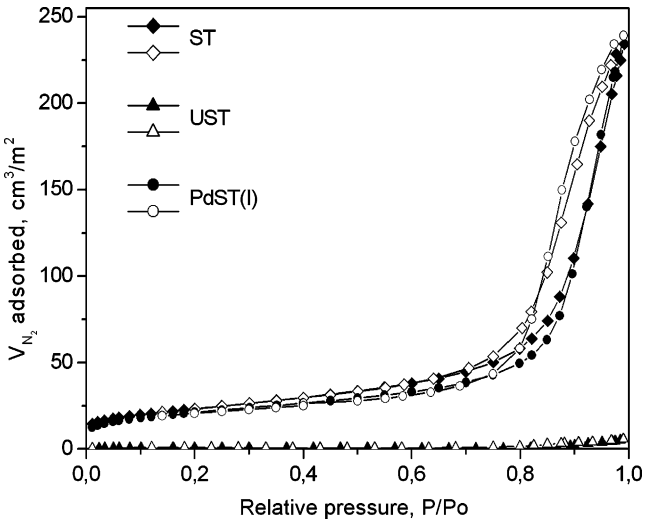

Fig. 2. Nitrogen adsorption isotherms of ST, UST and PdST(I) (filled symbols indicate adsorption, open symbols indicate desorption).

volume (0.007 cm^3/g) than sulphated ones. According to IUPAC classification, type IV isotherms and type H3 hysteresis loops are observed for sulphated titania materials. Besides their average pore sizes are between 15.9–19.9 nm. Therefore, the addition of H_2SO_4 during gellation step lead to mesoporous materials. In all cases the *C* constant from BET equation is in the range 119–179 confirming that BET model is in the optimal range of application ($50 < C < 200$) [14].

3.1.3. Chemical composition

Table 1 also shows results of X-ray fluorescence analysis of sulphated titania catalysts prepared by impregnation and cogellation. Pd composition deviates from the nominal content (0.5 wt.%), while Ni composition is close within experimental error to about 0.5 wt.%. Sulphur contents of PdST(I), NiST(I) and ST catalysts are found to be around 0.75 wt.% indicating that the sol–gel method followed in this work was reliable to prepare catalysts with similar sulphur loadings.

The oxidation state of Ni and Pd could not be established since the metal loading is quite low and the signal-to-noise ratio of the XPS spectra prevents any conclusion. In addition, decomposition processes associated to the presence of sulphate species (see Section 3.1.5) makes it difficult to determine metal oxidation state on the basis of hydrogen consumption by conventional TPR experiments**.** It is also difficult to know metal oxidation state during reaction due to the presence of oxidizing and reductant species (O_2, H_2O, Cl_2, HCl). In this work the assumption of metallic particles while reasonable is purely formal since changes in the oxidation state along the reaction path might be expected.

3.1.4. NH_3-TPD with DRIFTS

Surface species formed as a result of NH_3 adsorption were studied by DRIFTS. Fig. 3a shows infrared spectra taken over ST during TPD in flowing He. This way, positive bands indicate adsorbed species appearing upon ammonia adsorption while negative bands correspond to spectral features disappearing upon ammonia adsorption [15]. A band at 1178 cm^{-1} due to NH_3 adsorption on Lewis acid sites is observed. This band corresponds to $\delta_{as}(NH_3)$ vibrations of coordinative adsorbed ammonia [16]. NH_3 adsorption on Brönsted acid sites generated by sulphation is observed at 1464 and 1618 cm^{-1}. These bands represent asymmetric and symmetric deformation of ammonium ions (NH_4^+), respectively. Negative bands (1300, 1350 and 1600 cm^{-1}) are also seen in Fig. 3a. Yang et al. [16] assigned bands at 1300 and 1350 cm^{-1} to displacement of sulphate species on the surface while 1600 cm^{-1} band was associated with displaced hydroxyl groups on the surface. NH_3 was more strongly adsorbed on the surface than some of the hydroxyls and sulphate species. Features observed in the range 2800–3600 cm^{-1} correspond to N–H stretching vibrations of adsorbed NH_3 species. When ST was heated under He after NH_3 adsorption, band intensities of Brönsted acid sites on ST did not significantly decrease. So, Brönsted acid sites were relatively stable, at least up to 623 K.

The same experiment was performed on PdST(I), NiST(I) and UST. The spectra are presented in Fig. 3b–d, respectively. Compared to ST, band at 1641 cm^{-1} in spectra of PdST(I) and NiST(I) due to adsorbed NH_4^+ species decreases during heating in flowing He. In addition, spectra of NiST(I) exhibits a band at 1221 cm^{-1} showing the splitting of symmetric deformation mode of NH_3 which suggests that adsorption of molecular NH_3 was stronger on NiST(I) than on ST and PdST(I) [17].

Dissociative adsorption of NH_3 on UST, Fig. 3d, is evidenced by the appearance of a band at 1256 cm^{-1} assigned to dissociated ammonia forms [18]. Ammonia dissociation appears to generate Brönsted acidity, detectable by a band at 1458 cm^{-1}. Indeed, this band decreases in parallel with the disappearance of dissociated ammonia upon heating in flowing He. NH_3 adsorption on hydroxyl groups on the surface of UST are characterized by a broad band at 3228 cm^{-1}.

It is well accepted that Brönsted acidity plays a key role in determining the activity of acidic catalysts since the oxidation of chlorinated hydrocarbons is initiated by hydrocarbon adsorption on these sites [19]. Results of present ammonia TPD with DRIFTS experiments confirm that sulphate species remain on the surface of sulphated catalysts after heating to about 623 K. Sulphate species contribute to generate a large amount of Brönsted acid sites on sulphate promoted oxide samples, and these acid sites are very important for adsorption of organochlorinated compounds in oxidation reactions. They adsorb over acid sites by hydrogen bonds between chlorine and surface proton [20]. In contrast, when nitric acid is used as hydrolysis catalyst during sol–gel preparation, nitrate ion is volatized by calcination (4 h at 873 K) and only hydroxyl groups remain on UST surface.

3.1.5. Sulphate stability

Fig. 4 shows DTG of ST, PdST(I) and NiST(I) catalysts. The first weight loss at temperatures below 473 K corresponds to removal of water. A loss of mass between 473–573 K, is ascribed to carbonaceous residues remaining after calcination, while the last weight loss due to sulphate decomposition results in a maximum in the DTG at around 750 K. Evolving sulphur oxides have not been analyzed but both SO_2 and SO_3 might be expected, although the oxidizing character of the atmosphere

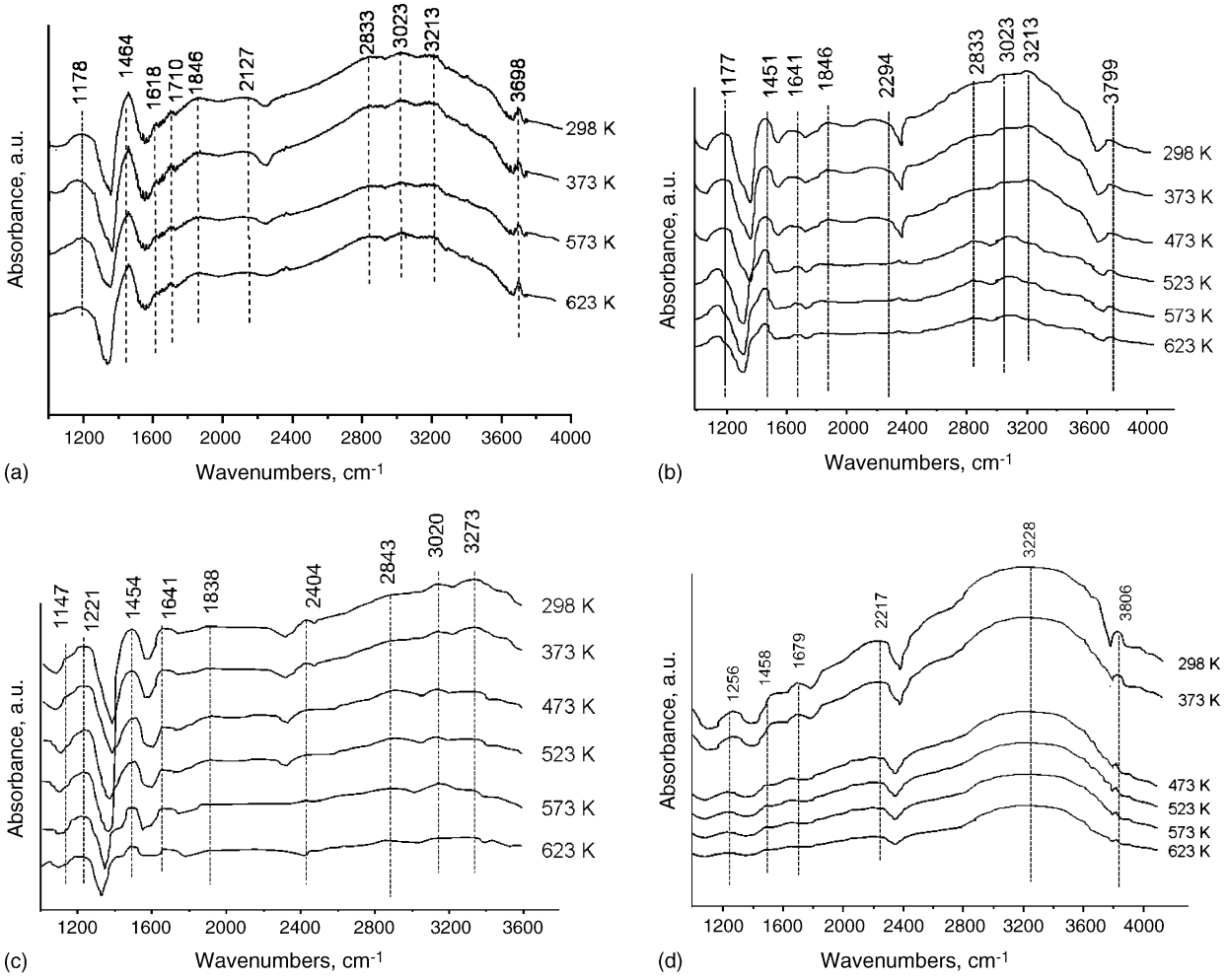

Fig. 3. NH_3-TPD with DRIFTS of: (a) ST; (b) PdST(I); (c) NiST(I); (d) UST.

and the presence of Ni or Pd should favour the evolution of sulphur trioxide. Weight loss changes in this region depend upon drying conditions and the amount of SO_4^{-2} added. Sulphate species on unmodified ST samples (sulphur lost above 873 K) were more stable than those over Pd and Ni modified samples (sulphur lost above 673 K) suggesting that Pd and Ni catalyzed sulphate decomposition.

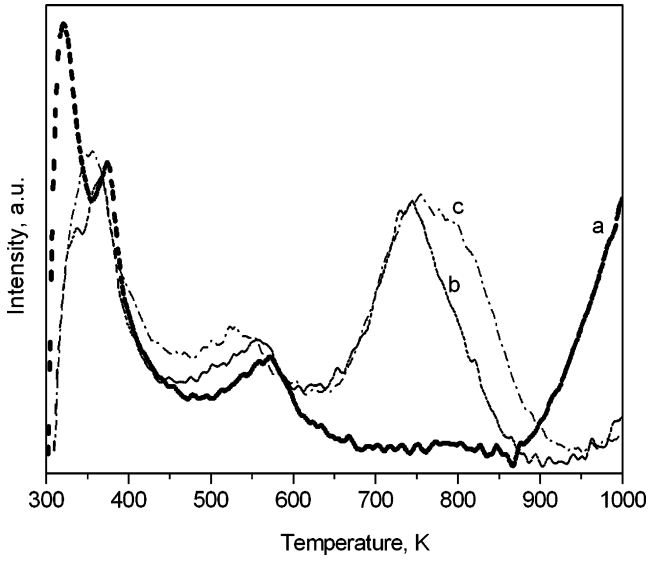

Fig. 4. DTG of: (a) ST; (b) PdST(I); (c) NiST(I).

3.1.6. Transmission electron microscopy (TEM)

Fig. 5a and b show TEM photographs of PdST(I) and PdST(C), respectively. Titania microstructure does not allow enough contrast to distinguish Pd. Only Ti, O, and S are detected by EDX indicating that Pd particles were very small. It is observed that PdST(I) prepared by impregnation (Fig. 5a) possesses uniform, finely distributed ST particles. However, particles of PdST(C) samples prepared by cogellation are clamped to each other forming agglomerates (Fig. 5b).

3.2. Activity tests

Fig. 6 shows conversion profiles as a function of temperatures (light-off curves) for sulphated support and modified (impregnated and cogelled) sulphated catalyst samples compared to that obtained under thermal conditions. As shown in Fig. 6, the homogeneous reaction started above 623 K and a temperature of 773 K was required to obtain 20% conversion. This is in agreement with results by Windawi and Zhang [21]

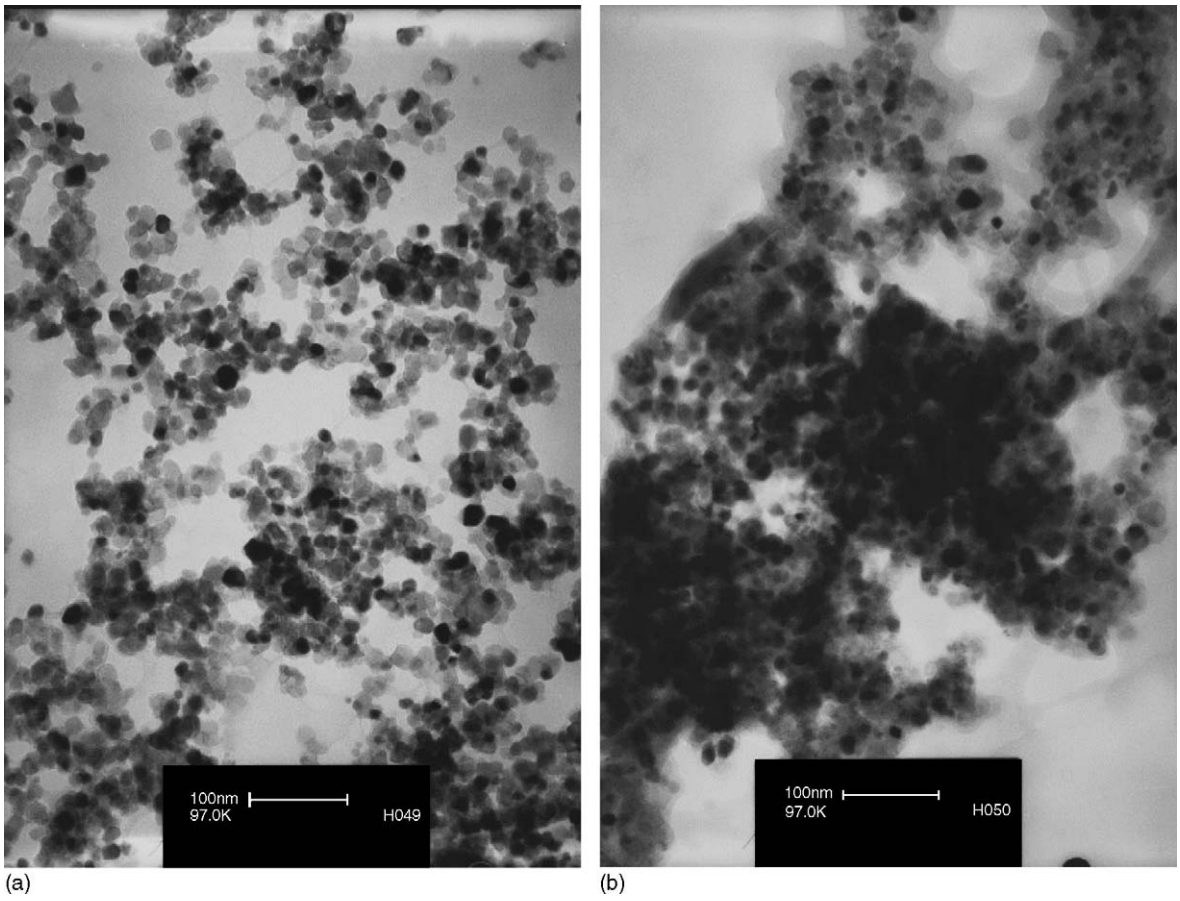

Fig. 5. Transmission electron microscopy (TEM) of: (a) PdST(I); (b) PdST(C).

who observed homogeneous reaction beyond 673 K. Catalytic destruction of DCM depends on preparation method, i.e. when metal precursor is added during gellation step, metallic phase is not easily accessible to reactants. Under the conditions of this work, impregnated catalysts exhibited higher activity than those prepared by cogellation. Temperatures at which 50% conversion was achieved, T_{50}, were 530, 528, 535 K over NiST(I), PdST(I) and ST, respectively. Interestingly, the unmodified ST support exhibited comparable activity to that obtained over Ni and Pd modified sulphated catalysts showing that Brönsted acid sites play a crucial role in the destruction of DCM. The T_{50} value obtained over ST was much lower than that previously obtained over protonic zeolites at a much lower W/F (0.0017 g min mL^{-1}) and under dry conditions [22]. The T_{50} values of cogelled catalysts were 603 and 633 K over PdST(C) and NiST(C), respectively.

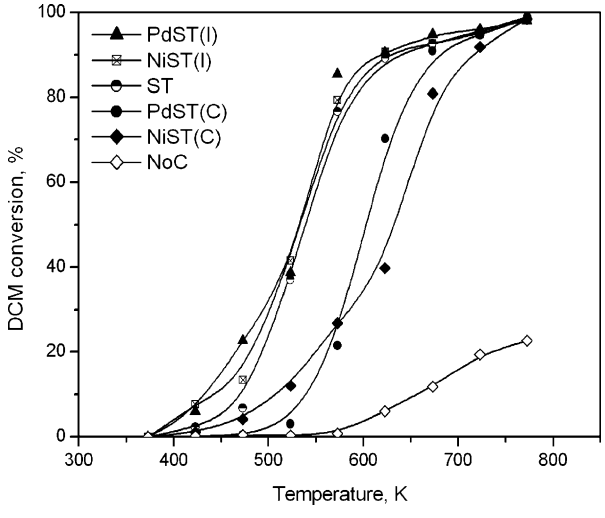

Fig. 6. Light-off curves of DCM oxidation over impregnated and cogelled sulphated titania catalysts and homogeneous reaction (NoC).

Fig. 7 compares light-off curves of homogeneous reaction and of sulphated, PdST(I), NiST(I), and un-sulphated, PdUST(I), NiUST(I) samples. The presence of SO_4^{-2} enhanced DCM oxidation. $T_{50\%}$ was 648 K for PdUST(I) and 528 K for PdST(I). Although the effect of surface area and relative proportion of anatase phase can not be separated, enhanced activity at low temperatures exhibited by sulphated catalysts for DCM oxidation compared to un-sulphated ones is ascribed to acidity. Our previous results on zirconia-supported catalysts prepared by sol–gel method confirm the above statement [11]. Therefore, bifunctional catalysts are required for DCM combustion in the presence of water vapour at relatively low temperature.

Figs. 8–10 show the light-off curves and observed product distribution for NiST(I), PdST(I) and ST catalysts, respectively. As described above, light-off curves for DCM oxidation over NiST(I), PdST(I) and ST overlap having almost the same T_{50}

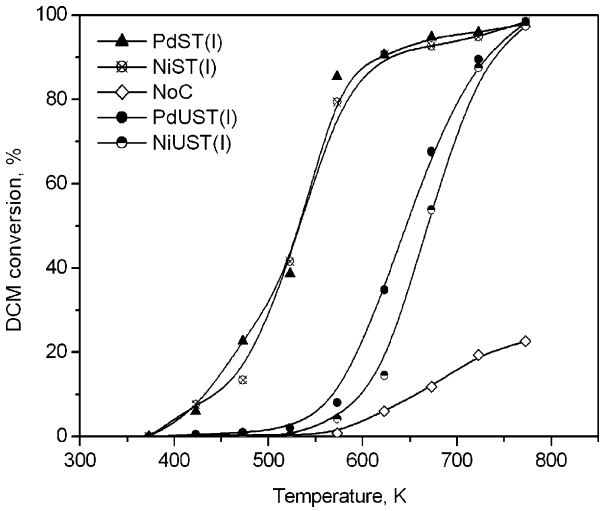

Fig. 7. Light-off curves of DCM oxidation over impregnated Pd and Ni modified sulphated and un-sulphated titania, and homogeneous reaction (NoC).

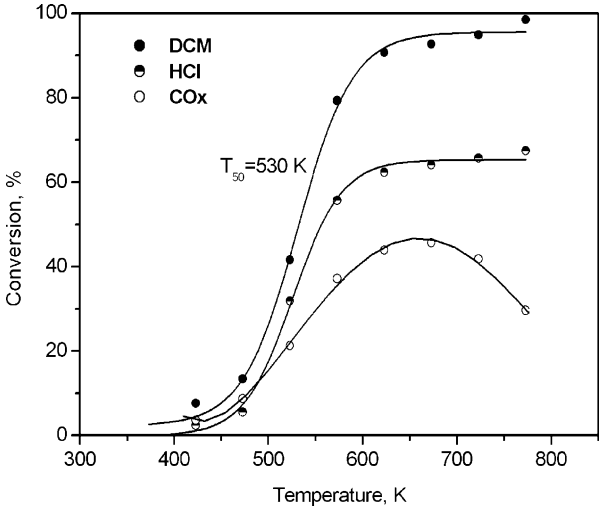

Fig. 8. Light-off curves for the oxidation of DCM and observed product distribution over NiST(I).

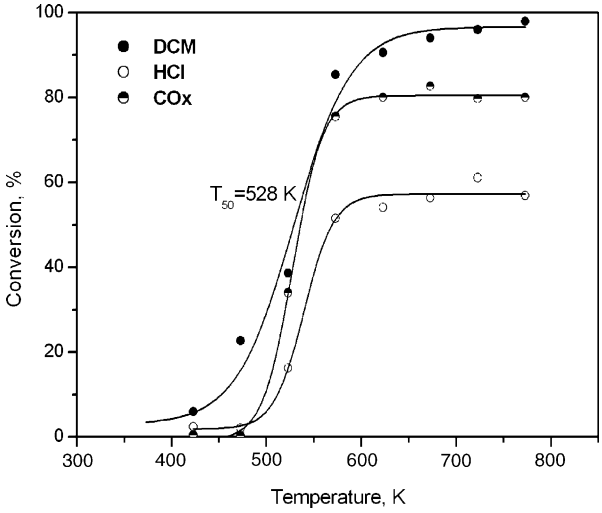

Fig. 9. Light-off curves for the oxidation of DCM and observed product distribution over PdST(I).

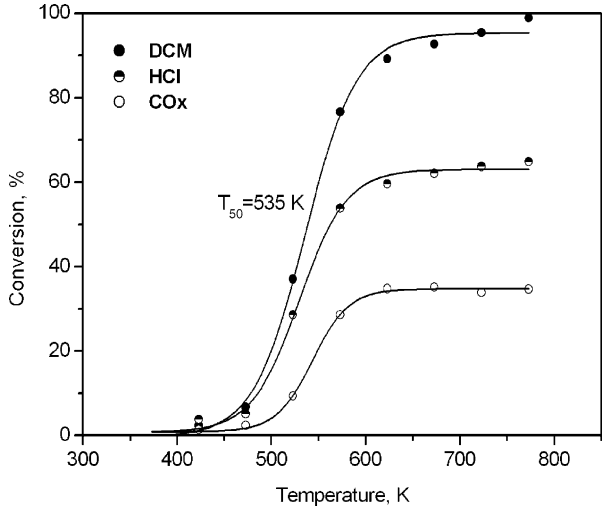

Fig. 10. Light-off curves for the oxidation of DCM and observed product distribution over ST.

value. The main oxidation products from DCM decomposition over NiST(I) and ST were HCl and CO (DCM conversion to CO_2 was lower than 0.1%), while the contribution to CO_x species from CO_2 was favoured over PdST(I). In this case, DCM conversion to CO was always lower than 1%. For NiST(I) and ST DCM conversion to HCl was practically the same. Only a small increase in CO conversion values was detected for NiST(I) catalyst in the temperature range studied. At temperatures lower than 523 K DCM conversion is slightly higher for NiST(I) than ST, but at higher temperatures differences in total conversion and HCl production are hardly observable. Yang and Hlavacek [23] have studied the chlorination of titanium oxide with gaseous chloride in the presence of carbon. From their studies it is clear that TiO_2–C–Cl complex between 423 and 723 K can be formed and total conversion of this complex can occur at 623 K. Under reaction conditions of this work the light-off curves shown in Fig. 10 are explained on the basis of the formation of titanium chloride at temperatures higher than 423 K and once this phase is formed the catalyst behaves exactly like catalysts impregnated with Ni showing selective formation of HCl.

Pinard et al. [24–26] demonstrated that for oxidation of chlorinated hydrocarbons in the presence of water over Pt zeolites both protonic and platinum sites are required (reaction (3)):

$$CH_2Cl_2 + O_2 \rightarrow CO_2 + HCl \quad (3)$$

Reactions (4) and (5) indicate a bifunctional mechanism involving DCM hydrolysis on the support and oxidation of the hydrolyzed products at metal sites [24–26]:

$$CH_2Cl_2 + H_2O \rightarrow HCHO + 2HCl \quad (4)$$

$$2HCHO + O_2 \rightarrow 2CO + 2H_2O \quad (5)$$

$$2CO + O_2 \rightarrow 2CO_2 \quad (6)$$

If the studied reaction follows the mechanism proposed by Pinard et al. [24–26] the conversion to HCl and CO_x should be the same. As can be observed in Figs. 8 and 9, CO_x (mainly CO) concentration is lower than HCl concentration for NiST(I) and

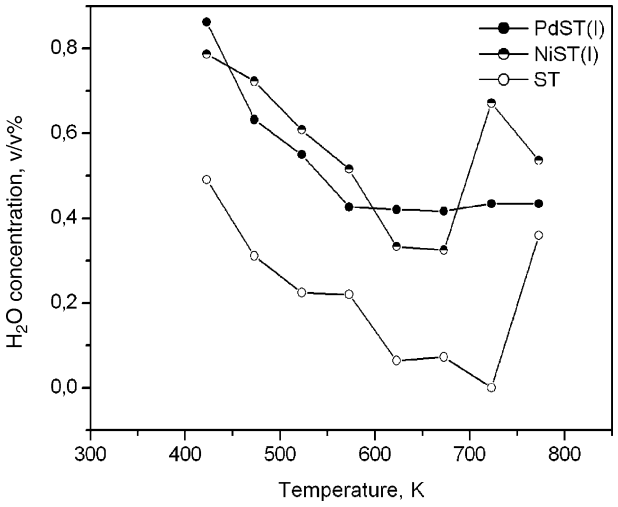

Fig. 11. Evolution of water concentration during DCM oxidation over PdST(I), NiST(I) and ST.

ST in the temperature range studied which necessarily should result in the formation of a carbonaceous layer on these catalysts.

It has been observed that water plays an important role in the catalytic oxidation of chlorinated hydrocarbons [27]. In this work, runs carried out without water vapour in the feed stream (not shown) lead to slightly lower conversion in comparison to those runs in which 1% water was fed. When no water was introduced in feed stream $T_{50\%}$ value was 653 K over PdST(I), chlorine was retained on catalyst since little conversion to HCl was observed and CO was also favoured together with small amounts to CO_2. Water is believed to remove chlorine from the surface of noble metal catalysts affecting activity [27]. Water can regenerate the surface with H^+ and OH^- species that constitute Brönsted acid sites, which are necessary in oxidation reactions. Protons can be recombined with chlorine favouring formation of higher amount of hydrogen chloride [28].

Fig. 11 shows the evolution of H_2O as a function of temperature for DCM oxidation over PdST(I), NiST(I) and ST during the course of the reaction. In general, there is a decrease in water concentration and a further increase as a result of the decomposition of intermediate products and the combustion of the carbonaceous residues for NiST(I) and ST. In the case of PdST(I) water concentration decreases. The decrease in water concentration may favour Deacon reaction (7) reducing selectivity towards HCl.

$$2HCl + O_2 \rightarrow Cl_2 + H_2O \quad (7)$$

Following the mechanism proposed by Liu et al. [29] for the interaction of CCl_4 with titania surface, DCM may interact with the surface dissociating chlorine atoms, that should adsorb on defective titanium ions, and the CH_2 group which might sit on surface oxide ions. This situation should lead to the formation of intermediate HCHO species that further react with the catalyst surface resulting in CO_x species. The oxygen vacancy left by the formation of the intermediate will be occupied by a formal Cl_2^{2-} ion resulting from the adsorption of the two chlorine atoms leading to the formation of a Ti–Cl–Cl–Ti bridge that in the presence of dry oxygen should evolve either as Cl_2 (Deacon reaction) recovering the vacancy left behind with an oxide ion or as two HCl molecules, when water is present. In the case of nickel catalysts the CH_x residue would result, even at low temperature, in the formation of carbon whiskers making the metallic surface inaccessible to DCM molecules and showing identical behaviour to that of the sulphated support, except for small differences in the evolution of carbon oxides that is obviously influenced by the excess carbon. The higher reactivity of Pd surfaces should result in water dissociation and hence hydrogen spillover would result in higher HCl conversion and total oxidation of carbon residues.

4. Conclusions

Results from this work allow us to draw several interesting conclusions as regards to the influence of hydrolysis catalyst (H_2SO_4 or HNO_3), preparation (impregnation or cogellation) and metallic phase (Pd or Ni) on physicochemical properties and reactivity of xerogel titania catalysts for DCM oxidation:

- After calcination nitrate ion is volatized from UST and only hydroxyl groups remain on its surface. On the other hand, sulphate ions remain on the surface of catalyst prepared using sulphuric acid as hydrolysis catalyst and promote the formation of Brönsted acid sites.
- Only Pd impregnated catalyst samples are effective for deep DCM oxidation since metallic phase may not be accessible when xerogel sulphated titania is modified with Pd by cogellation.
- The unmodified xerogel sulphated titania support and that modified with Ni exhibited similar oxidation activity but, formation of CO was favoured suggesting that the type of metal species is crucial for total combustion of DCM.
- The highly active performance of xerogel sulphated titania supported samples for DCM oxidation could be accounted for by the generation of strong acid sites, which were preferentially Brönsted sites and the presence of Pd appear to be essential for DCM decomposition into CO_2 and HCl.

Acknowledgements

L.M. Martínez T and C. Montes de Correa would like to thank Colciencias and Universidad de Antioquia for financial support of this work through project Cod 1115-05-12426. L.M. Martínez T is grateful to UdeA for supporting her stay at the “Instituto de Ciencia de los Materiales Universidad de Sevilla-CSIC”, Sevilla, Spain.

References

[1] E. Ortiz-Islas, R. Gómez, T. López, J. Navarrete, D.H. Aguilar, P. Quintana, Appl. Surf. Sci. 252 (2005) 807.
[2] B.M. Reddy, I. Ganesh, A. Khan, J. Mol. Catal. A 223 (2004) 295.
[3] J.A. Wang, A. Cuan, J. Salmones, N. Nava, S. Castillo, M. Morán-Pineda, F. Rojas, Appl. Surf. Sci. 230 (2004) 94.
[4] Y. Li, B. Xu, Y. Fan, N. Feng, A. Qiu, J. He, H. Yang, Y. Chen, J. Mol. Catal. A 216 (2004) 107.

[5] S.M. Jung, P. Grange, Appl. Catal. B 36 (2002) 207.
[6] D.J. Suh, T.J. Park, Chem. Mat. 8 (1996) 509.
[7] L.A. Contreras, J.L.R. Cerda, Actas do XVII Simposio Iberoamericano de Catálise, Julio 16–21, 2000, p. 205.
[8] L. Castro, P. Reyes, C. Montes de Correa, J. Sol–Gel Sci. Tech. 25 (2002) 159.
[9] V.I. Pârvulescu, V. Pârvulescu, U. Endruschat, Ch.W. Lehmann, P. Grange, G. Poncelet, H. Bönnemann, Microp. Mesop. Mat. 44/45 (2001) 221.
[10] B.D. Cullity, Elements of X-Ray diffraction, 2nd ed., Addison Wesley Publishing Company, Inc, 1978, p. 284.
[11] L.M. Martinez, C. Montes de Correa, J.A. Odriozola, M.A. Centeno, Catal. Today 107/108 (2005) 800.
[12] B.C. Lippens, J.H. DeBoer, J. Catal. 4 (1965) 319.
[13] S.K. Samantaray, T. Mishra, K.M. Parida, J. Mol. Catal. A 156 (2000) 267.
[14] G. Leofanti, M. Padovan, G. Tozzola, B. Venturelli, Catal. Today 41 (1998) 207.
[15] M.A. Centeno, I. Carrizosa, J.A. Odriozola, Appl. Catal. B 19 (1998) 67.
[16] R.T. Yang, W.B. Li, N. Chen, Appl. Catal. A 169 (1998) 215.
[17] J.M. Watson, U.S. Ozkan, J. Mol. Catal. A 192 (2003) 79.
[18] K. Hadjiivanov, Appl. Surf. Sci. 135 (1998) 331.
[19] R. López-Fonseca, B. de Rivas, J.I. Gutiérrez-Ortiz, A. Aranzábal, J.R. González-Velasco, Appl. Catal. B 41 (2003) 31.
[20] M.A. Gómez, W.L. Vargas, Rev. Colombiana Ing. Quím. 27 (1998) 61.
[21] H. Windawi, Z.C. Zhang, Catal. Today 30 (1996) 99.
[22] X.Z. Jiang, L.Q. Zhang, X.H. Wu, L. Zheng, Appl. Catal. B 9 (1996) 229.
[23] F. Yang, V. Hlavacek, React. Kin. Catal. 46 (2000) 356.
[24] L. Pinard, J. Mijoin, P. Magnoux, M. Guisnet, J. Catal. 215 (2003) 234.
[25] L. Pinard, P. Magnoux, P. Ayrault, M. Guisnet, J. Catal. 221 (2004) 662.
[26] L. Pinard, J. Mijoin, P. Ayrault, C. Canaff, P. Magnoux, Appl. Catal. B 51 (2004) 1.
[27] G.C. Bond, C.F. Rosal, Catal. Lett. 39 (1996) 261.
[28] J.R. Gonzalez-Velasco, A. Aranzábal, J.I. Gutierrez-Ortiz, R. López Fonseca, Appl. Catal. B 19 (1998) 189.
[29] G. Liu, J. Wang, Y. Zhu, X. Zhang, Phys. Chem. Chem. Phys. 6 (2004) 985.